Crack Nucleation in Phase Field Fracture Models

Charlotte Kuhn[1,*], Ralf Müller[1]

[1] Institute of Applied Mechanics, TU Kaiserslautern, P.O.B. 3049, 67653 Kaiserslautern, Germany
* Corresponding author: chakuhn@rhrk.uni-kl.de

Abstract Phase field fracture models are able to reproduce a wide range of phenomena, which are observed in fracture experiments. These phenomena include the nucleation of new cracks in initially undamaged material. However, none of the material parameters of a phase field fracture model is directly connected to the fracture strength of the material. Thus, the critical stress for the nucleation of new cracks is not a priori clear. Crack nucleation in a phase field fracture model is preceded by a localization of the initially homogeneous crack field in an area surrounding the nucleating crack. For homogeneous problems, it can be shown analytically that the onset of the localization is caused by the loss of stability of the crack-free homogeneous solution of the phase field equations at a certain load level. This critical stability load provides a definition of the fracture stress in the phase field model depending on the stiffness of the material, the cracking resistance and the internal length of the phase field model. The analytical findings are illustrated in finite element simulations of the phase field fracture model. Further numerical investigations analyze the crack nucleation behavior of the phase field model in more complicated scenarios, where analytical stability results are not available.

Keywords Phase field model, Fracture, Finite element method, Crack nucleation, Stability

1. Introduction

Conclusions drawn from numerical simulations often play a crucial role in the design process of structural components. In order to obtain a reliable prediction of the integrity of a structure, a fracture model must be able to reproduce a wide range of phenomena which are observed at fracture events. On the one hand, this requires criteria for the stability of pre-existing cracks as well as criteria for the nucleation of new cracks in originally undamaged material. On the other hand, the fracture model must also predict the geometry of the crack path, including possible kinking of a crack or bifurcation into several crack branches. Unlike many other continuum fracture models, which are equipped with a whole toolbox of different criteria in order to meet these requirements, the phase field approach provides a unified framework for the simulation of the entire fracture process. Different phase field fracture models have been introduced and discussed e.g. in references [1–6]. More recently, phase field fracture models based on Bourdin's regularization of the variational formulation of brittle fracture [7] have been formulated in [8–10]. All these models differ in detail, but in all formulations cracks are represented by a scalar phase field order parameter, which indicates the condition of the material and interpolates smoothly between broken and undamaged material. Cracking is addressed as a phase transition problem, and the crack evolution, obtained implicitly through the solution of the coupled field equations, covers the whole range of phenomena which need to be considered. Concerning a finite element implementation of the fracture model, the phase field approach is advantageous because the diffuse phase field cracks do not lead to discontinuous jumps in the displacement field. Thus, the discretization can be done with standard finite element shape functions, and no remeshing is required in order to simulate crack propagation.

The fracture behavior of phase field fracture models is mainly adjusted by two parameters. The cracking resistance $\mathcal{G}_c$ is a material parameter, which is a measure for the surface or fracture energy, needed to create new fracture surfaces. By means of configurational forces, it can be illustrated, that the propagation of pre-existing cracks in the phase field model agrees with the energetic considerations of classical Griffith theory, see e.g. [8, 11, 12]. The second parameter is a length

scale ξ, which primarily controls the width of the transition zone of the order parameter between broken and undamaged material. From this point of view, the length scale is merely an auxiliary numerical quantity, which recovers the sharp interface limit for $\xi \to 0$. However, some recent publications [13–16] find that, in a one dimensional setting, the length scale ξ is also crucial for the stability of crack-free, spatially homogeneous phase field solutions. At the critical load level, the crack-free solution becomes unstable and the phase field order parameter localizes until finally a crack forms. Particularly interesting is the fact, that this stability point is also related to the maximal stress response of the crack-free phase field solution. This observation allows for the definition of a fracture strength in the phase field model, which – at first sight – does not feature a material parameter, that is directly connected to the strength of the material, but is able to reproduce crack nucleation.

In this work, the crack nucleation behavior of the phase field fracture model introduced in [8] is investigated. In a first step, only the one dimensional case is considered. A stability analysis of the spatially homogeneous, crack-free solution is outlined, which yields the definition of an effective fracture strength in the one dimensional phase field model. In a second step, the problem of crack nucleation is considered in the two dimensional setting. However, a rigorous analytical stability analysis is generally not possible in the case of arbitrary inhomogeneous stress states. Therefore, based on the findings from the one dimensional case, strength estimates are derived for the two dimensional setting. These estimates are then compared to the computed stress states at crack nucleation in a finite element simulation of the phase field model.

2. Phase field formulation

In phase field fracture models, cracks are approximated by the zero set of the phase field order parameter s. This order parameter is a continuous scalar field quantity which resembles a damage variable and is often referred to as crack field in this context. It interpolates smoothly between cracks, where the order parameter takes the value zero, and undamaged material, where the value of the order parameter is one. By means of a degradation function, the crack field is coupled to the elastic stiffness tensor $\mathbb{C}$ of the material in order to model the change in stiffness between broken and undamaged material. The core of the phase field model considered in this work is the energy density functional

$$\psi(\varepsilon, s) = \frac{1}{2}(s^2 + \eta)\varepsilon : \mathbb{C}\varepsilon + \mathcal{G}_c \left(\frac{(1-s)^2}{4\xi} + \xi |\nabla s|^2 \right), \tag{1}$$

which was introduced by Bourdin [7] as a regularized approximation of the energy density of a linear elastic fractured body. The first part, which is a function of the linearized strain tensor ε and the crack field s, is the elastic stored energy. The small positive parameter $\eta \ll 1$ in the degradation function is a residual stiffness, which is introduced in order to avoid numerical difficulties, where s equals zero. The second part depends only on the crack field s and its gradient ∇s. An integration of the second bracketed term over the entire domain yields an approximation of the surface measure of the crack set, when the regularization length ξ is sufficiently small. Multiplied with the cracking resistance $\mathcal{G}_c$ it approximates the Griffith type surface energy of the crack set. By virtue of thermodynamic reasoning, the definition of the energy density functional ψ yields the material law

$$\sigma = \frac{\partial \psi}{\partial \varepsilon} = (s^2 + \eta)\mathbb{C}\varepsilon \tag{2}$$

for the stress tensor σ which, together with the equilibrium condition

$$\operatorname{div} \sigma = 0 \tag{3}$$

and the respective boundary conditions, forms the mechanical part of the problem. The evolution of the crack field is assumed to follow a Ginzburg-Landau type evolution equation, where the rate $\dot{s}$ is proportional to the negative variational derivative of the energy density functional with respect to s, i.e.

$$\dot{s} = -M\frac{\delta\psi}{\delta s} = -M\left(s\varepsilon:\mathbb{C}\varepsilon - \mathcal{G}_c\left(2\xi\Delta s + \frac{1-s}{2\xi}\right)\right). \tag{4}$$

The symbol Δ denotes the Laplace operator. The positive scalar kinetic coefficient M describes the mobility of the process. In the format of Eq. (4), the evolution equation may be regarded as a viscous approximation of the quasi-static case, which is recovered for $M \to \infty$. In order to model the irreversibility of the fracture process, Dirichlet boundary conditions $s = 0$ are applied to the crack field in the subsequent load steps, wherever a crack forms, i.e. the crack field becomes zero. At crack free boundaries with outer normal vector n, homogeneous Neumann boundary conditions $\nabla s \cdot n = 0$ apply. The coupling of the field equations (Eqs. 2-4) implicitly models the mutual interaction between the elastic stress and strain fields and the crack field s. Given a prescribed loading history, the successive solution of the coupled system of equations formed by Eqs. (2-4) yields the evolution of the mechanical stress and strain fields as well as the evolution of the crack field. Note, that no further criteria are required in order to capture even complex crack evolutions, such as the coalescence of different cracks, crack branching or the nucleation of new cracks.

3. Crack nucleation

The nucleation of new cracks in an originally undamaged structure is a somewhat delicate topic in the context of a phase field formulation. On the one hand, crack nucleation can be observed in numerical simulations of the phase field model. On the other hand, none of the parameters of the phase field fracture model is directly connected to the fracture strength σ_c of the material. In the following, the influences of the different phase field parameters on the effective fracture strength of the phase field model are investigated by means of an analytical stability analysis and numerical simulations.

3.1. The one dimensional case

3.1.1. Homogeneous solution

In a first step, a one dimensional problem is considered. A homogeneous bar of length $2L$ and Young's modulus E is strained by an increasing displacement load of $u(\pm L) = \pm u_0$ at both ends. Before any load is applied, the bar is modeled as undamaged, i.e. $s \equiv 1$. In the one dimensional setting, the equilibrium condition (Eq. 3) immediately implies that the stress σ must be constant along the entire bar. Under the assumption that the crack field remains spatially constant upon loading, it follows from the material law (Eq. 2, where Young's modulus E replaces the stiffness tensor $\mathbb{C}$) that the strain ε must be constant, too. The kinematic relation $\varepsilon = u'$ yields the strain value $\varepsilon_h = u_0/L$ prescribed by the boundary displacement. The corresponding static solution for the crack field

$$s(x) \equiv s_h = \frac{\mathcal{G}_c}{2\xi E\varepsilon_h^2 + \mathcal{G}_c} \tag{5}$$

is obtained from the one dimensional evolution equation. Accordingly, the constant stress in the bar is

$$\sigma_h = \frac{\mathcal{G}_c{}^2 E \varepsilon_h}{\left(2\xi E \varepsilon_h^2 + \mathcal{G}_c\right)^2}\,, \tag{6}$$

where the contribution of the remaining stiffness η has been neglected for the sake of algebraic simplicity. While the homogeneous crack field (Eq. 5) decreases monotonically with the increasing strain ε_h, the stress response (Eq. 6) attains a maximal value

$$\sigma_h^* = \frac{9}{16}\sqrt{\frac{\mathcal{G}_c E}{6\xi}}\,, \tag{7}$$

at a displacement load of

$$u_0^* = \sqrt{\frac{\mathcal{G}_c}{6\xi E}}\,L\,. \tag{8}$$

Interestingly, the value of the homogeneous crack field at the maximal stress load is *0.75*, independent of all of the phase field parameters, see also [10]. This is illustrated in the plots of Fig. 1, which show the evolution of the stress response and the crack field with respect to the displacement loading for different values of ξ.

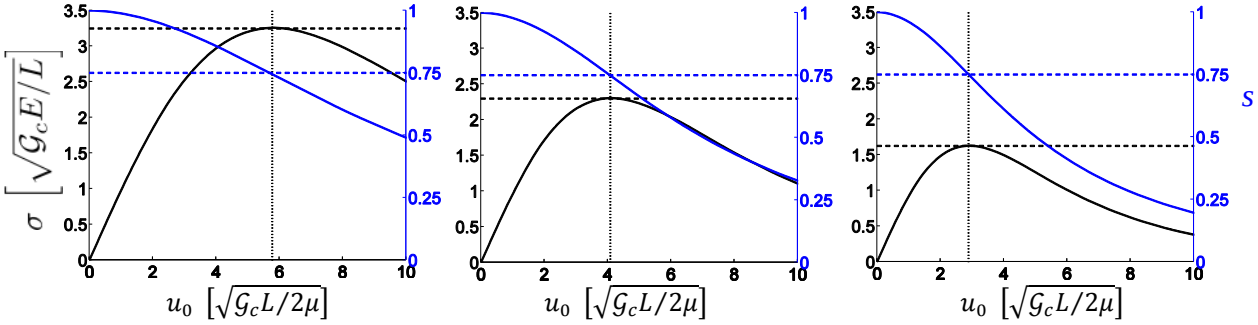

Figure 1. Stress response (black) and crack field (blue) under increasing displacement load for $\xi = 0.005L$ (left), $\xi = 0.01L$ (center) and $\xi = 0.02L$ (right)

3.1.2. Stability analysis

In order to analyze the stability of the homogeneous solution (Eq. 5), a family of symmetric test functions $s_\alpha(x) = s_\alpha(-x)$ with $s'_\alpha(\pm L) = s'_\alpha(0) = 0$ and $s_0(x) \equiv s_h$ is introduced. Symmetry is postulated for the sake of simplicity, and the restriction $s'_\alpha(0) = 0$ ensures differentiability at $x = 0$. Boundary conditions $u_\alpha(\pm L) = \pm u_0$, kinematic relations, the material law and the fact that the stress is constant yield the corresponding strain field ε_α. It can be shown that the first variation of the potential

$$\Pi(\varepsilon, s) = \int_{-L}^{L} \psi(\varepsilon, s)\,\mathrm{d}x = 2\int_0^L \psi(\varepsilon, s)\,\mathrm{d}x \tag{9}$$

vanishes for the homogeneous static solution, i.e.

$$\delta_\alpha \Pi(\varepsilon_\alpha, s_\alpha) = \frac{\mathrm{d}\Pi(\varepsilon_\alpha, s_\alpha)}{\mathrm{d}\alpha}\Big|_{\alpha=0} = 0\,. \tag{10}$$

Thus, the homogeneous solution is always a local extremum or a saddle point of the energy functional (Eq. 9). The second variation of the potential Π with respect to α is given by the expression

$$\delta_\alpha^2\Pi = 2\left[4\frac{E}{L^3}u_0^2\left(\int_0^L \partial_\alpha s_\alpha \,\mathrm{d}x\right)^2 + 2\mathcal{G}_c\xi\int_0^L(\partial_\alpha s_\alpha')^2\mathrm{d}x + \left(\frac{\mathcal{G}_c}{2\xi}-\frac{3E}{L^2}u_0^2\right)\int_0^L(\partial_\alpha s_\alpha)^2\mathrm{d}x\right], \quad (11)$$

where $\partial_\alpha(\cdot)$ denotes the partial derivative with respect to α. Clearly, the second variation can only become negative if the factor in front of the last integral in Eq. (11) becomes negative. If the displacement load u_0 is smaller than the load u_0^* (Eq. 8) with the maximal stress response, the second variation (Eq. 11) is positive. Thus, the homogeneous solution is a local minimizer of the total energy and therefore is considered as stable. If the displacement load u_0 becomes larger than the load u_0^*, the factor in front of the last integral becomes negative and thus, the second variation can become negative, too. The homogeneous solution is then no longer a local minimizer and becomes unstable. Consequently, the load with the maximal stress response represents a lower bound for the stability of the homogeneous solution. A further analysis of the stability of homogeneous solutions of different gradient damage formulations, is carried out in [16] and, for a broader class of gradient damage models, in [13–15]. Concerning the specific phase field fracture model under consideration, the main conclusion from these publications is, that for small values of ξ, the actual stability load lies slightly above the lower bound u_0^*. Only for rather large ξ, the actual stability load is significantly larger than u_0^*. However, regarding the regularizing character of ξ, this case is of minor interest.

3.1.3 Non-homogeneous solution

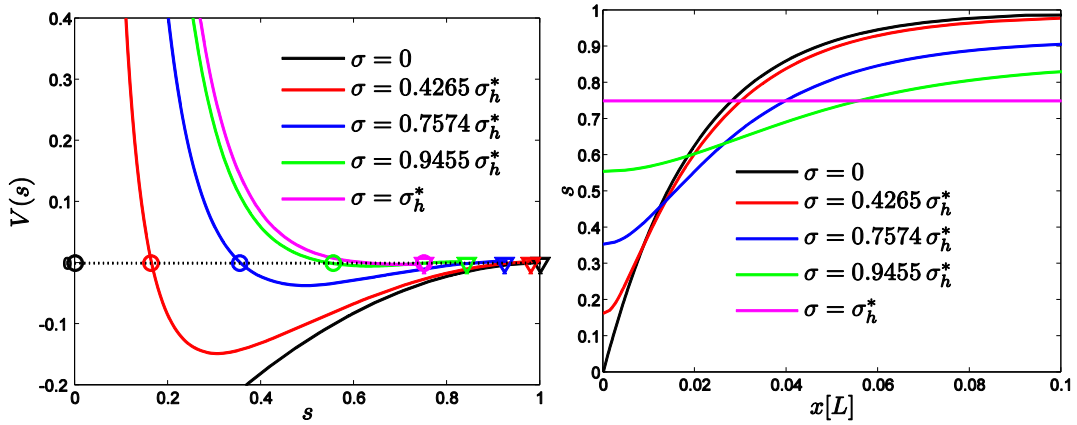

Figure 2. Function $V(s)$ and roots s_m (circles) and s_h (triangles) for different values of σ (left) and the respective inhomogeneous crack fields (right)

In this section, a semi-analytical approach to the computation of the non-homogeneous crack field at supercritical loading is outlined. More details are reported in [10, 11] for similar phase field models. A finite element study of the non-homogeneous solution stages can be found in [12]. The static one dimensional evolution equation (Eq. 4) and the material law (Eq. 2) can be recast in the format

$$\frac{2\xi\sigma^2 s}{\mathcal{G}_c E(s^2+\eta)^2} + s - 4\xi^2 s'' - 1 = 0\,. \quad (12)$$

Assuming a differentiable, symmetric solution $s(x)$ with a minimum value s_m at $x = 0$, an integration of Eq. (12) with respect to s over the interval $[s_m, s(x)]$ yields

$$\underbrace{2\xi^2(s')^2}_{V_{\mathrm{kin}}(s')} + \underbrace{\frac{\xi\sigma^2}{\mathcal{G}_c E(s^2+\eta)} - \frac{s^2}{2} + s}_{V_{\mathrm{pot}}(s)} = \underbrace{\frac{\xi\sigma^2}{\mathcal{G}_c E(s_m^2+\eta)} - \frac{s_m^2}{2} + s_m}_{V_{\mathrm{pot}}(s)}\,, \quad (13)$$

which can be interpreted as a balance law for the phase field variable s with the potential V_{pot} and

the kinetic energy V_{kin}, see [11]. With the far field boundary conditions $s'(\pm L) = 0$ and $s(\pm L) = s_h(\sigma)$, the minimum value s_m can be computed from Eq. (13) as a root of the function $V(s) = V_{\text{pot}}(s) - V_{\text{pot}}(s_h)$. The left plot in Fig. 2 shows the function $V(s)$ for different values of σ and $\xi = 0.01L$. The roots referring to $s = s_h$ are marked by triangles, and the roots referring to $s = s_m$ are marked by cycles. The extreme cases $\sigma = 0$ (black) and $\sigma = \sigma_h^*$ (magenta) require special consideration. For $\sigma = 0$ and the respective homogeneous crack field value $s_h = 1$, the function $V(s)$ is non-positive in the entire interval $[0, 1]$, and the root defining s_m vanishes. However, for $\sigma \to 0$, the root s_m of $V(s)$ approaches zero. Together with the fact that $\sigma = 0$ represents the cracked state, this consideration legitimates to set $s_m = 0$ in this case. If σ approaches the maximal value σ_h^*, the roots defining s_m and s_h collapse in a single point at $s = 0.75$.

Once the minimum value s_m has been determined, the balance law (Eq. 13) can be exploited to compute the solution $s(x)$ of Eq. (12), or rather the inverse

$$x(s) = \operatorname{sgn}(x) \int_{s_m}^{s(x)} \sqrt{\frac{2\xi^2}{V_{\text{pot}}(s_m) - V_{\text{pot}}(s)}}\, \mathrm{d}s \tag{14}$$

of the solution. The right plot of Fig. 2 shows the results of a numerical evaluation of Eq. (14) at different stress levels σ. The fully cracked solution (black) is virtually identical to the function

$$s(x) = 1 - \exp\left(\frac{-|x|}{2\xi}\right), \tag{15}$$

which is an approximation of the piecewise defined static solution of the stress free evolution equation with boundary conditions $s(0) = 0$ and $s'(\pm L) = 0$. The limit case with maximal stress response $\sigma = \sigma_h^*$ (magenta) yields the homogeneous solution $s \equiv 0.75$.

3.2. The two dimensional setting

3.2.1 Strength estimates from homogeneous test problems

As in the one dimensional setting, the length parameter ξ has a crucial impact on the fracture strength σ_c of the two dimensional phase field model. However, analytical solutions of non-homogeneous two dimensional problems are generally not available, and thus, a rigorous mathematical stability analysis cannot be carried out. In order to determine the fracture strength of the two dimensional model, relations between ξ and σ_c are derived on the basis of the two homogeneous problems depicted in Fig. 3.

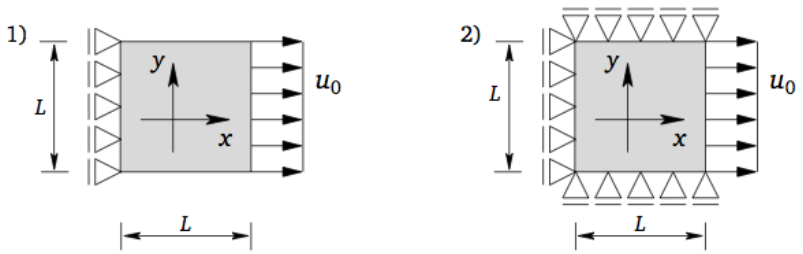

Figure 3. Homogeneous two dimensional problems for the derivation of strength estimates

For both cases, the stationary, homogeneous solution of the evolution equation is given by

$$s(x, y) \equiv s_h = \frac{\mathcal{G}_c}{2\xi\varepsilon : \mathbb{C}\varepsilon + \mathcal{G}_c}. \tag{16}$$

Due to the different boundary conditions, the elastic contribution differs slightly, depending on the ratio of the Lamé constants.

$$\varepsilon : \mathbb{C}\varepsilon = \kappa_i u_0^2 \qquad \text{with} \qquad \kappa_i = \begin{cases} \frac{2\lambda+2\mu}{\lambda+2\mu}, & \text{for } i = 1 \\ \frac{\lambda+2\mu}{2\mu}, & \text{for } i = 2 \end{cases} \tag{17}$$

The indices $i = 1, 2$ in Eq. (17) refer to the left and right setting depicted in Fig. 3. Neglecting η for algebraic simplicity, the corresponding stress in x-direction is

$$\sigma_x = \frac{2\mu\kappa_i \mathcal{G}_c{}^2 \varepsilon_x}{\left(4\mu\kappa_i \xi \varepsilon_x^2 + \mathcal{G}_c\right)^2} \tag{18}$$

with $\varepsilon_x = u_0/L$. The maximal value

$$\sigma_x^* = \frac{9}{16}\sqrt{\frac{2\mu\kappa_i \mathcal{G}_c}{6\xi}} \tag{19}$$

is attained at the displacement load

$$u_0^* = \sqrt{\frac{\mathcal{G}_c}{12\mu\kappa_i \xi}}\, L \,. \tag{20}$$

The maximal stress response (Eq. 19) and the corresponding displacement load (Eq. 20) exhibit the same asymptotic behavior with respect to ξ as in the one dimensional setting. For $\xi \to 0$ both quantities become infinitely large, while for $\xi \to \infty$ their value approaches zero. However, in the two dimensional setting, both quantities additionally depend on the factor κ_i defined in Eq. (17). As in the one dimensional case, the value of the homogeneous crack field at the maximal stress response is *0.75*, independent of all of the phase field model's parameters.

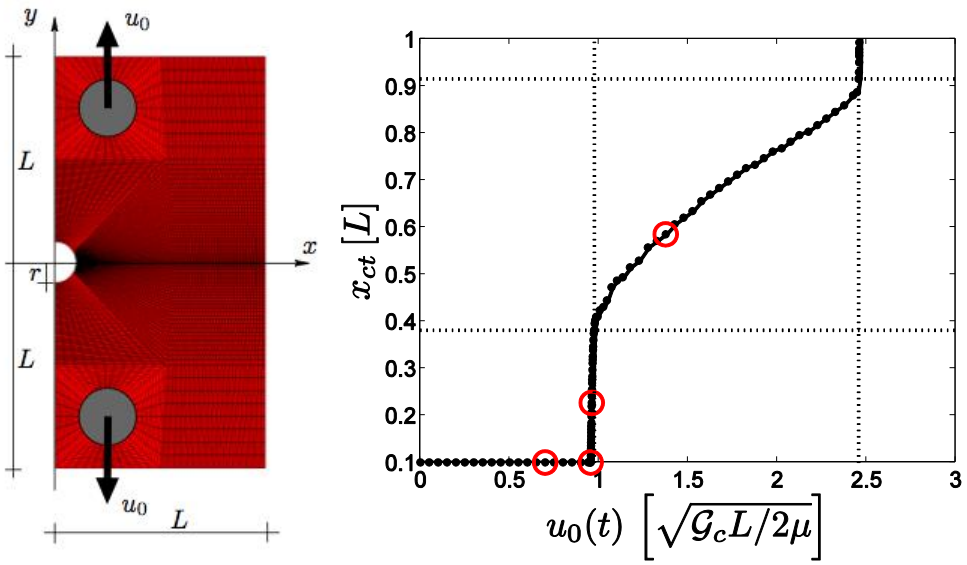

Figure 4. Simulation setup (left) and crack tip position with respect to the loading (right)

3.2.2 Numerical evaluation

In the following, the maximal stress values from Eq. (19) are compared to the actually computed stress states at crack nucleation in the phase field model, in order to evaluate the effective fracture strength σ_c of the phase field model. In the finite element simulation, the notched structure, depicted in the left plot of Fig. 4, is loaded by a linearly increasing displacement load $u_0(t)$ acting in y-

direction. The radius of the circular notch is $r = 0.1L$. The initial crack field is set to one in the entire domain in order to model the undamaged initial state. The material is assumed to be isotropic with Lamé constants $\lambda = \mu$, which is equivalent to a Poisson ratio of $\nu = 0.25$. The circular areas of diameter $d = 0.28L$ around the load application points (gray) are modeled as stiff by increasing the stiffness and the cracking resistance by a factor of *100*. The length parameter is $\xi = 0.01L$, the artificial residual stiffness in broken areas is set to $\eta = 10^{-5}$, and the kinetic coefficient is set to $M = 10\,L/\mathcal{G}_c T$, where the time scale T refers to the load factor t/T of the displacement load $u_0(t) = u_0(t/T)$. The size of the time steps is controlled by an adaptive time stepping procedure. More details on the finite element implementation of the phase field fracture model can be found in [8]. The right plot of Fig. 4 shows the position x_{ct} of the crack tip on the x-axis with respect to the displacement load (black solid line). For the evaluation the node with the largest x-coordinate where s equals zero is defined as the crack tip position. Before the onset of fracture, the crack tip position is replaced by the position of the notch ground located at $x = 0.1L$. After the critical load level is reached, an initial crack of finite length starting at the notch ground forms brutally along the x-axis at a quasi constant load level. The formation of the initial crack is followed by a phase of stable crack extension along the x-axis, where the crack grows progressively with the loading. A second phase of brutal crack extension is observed when total rupture occurs after the crack tip passes $x \approx 0.9L$. The dotted lines indicate the beginning and ending of the phase of stable crack growth. Remarkably, the crack nucleation at the non-singular stress concentration at the notch as well as the transition from brutal to stable crack extension and vice versa are mastered without any technical difficulties.

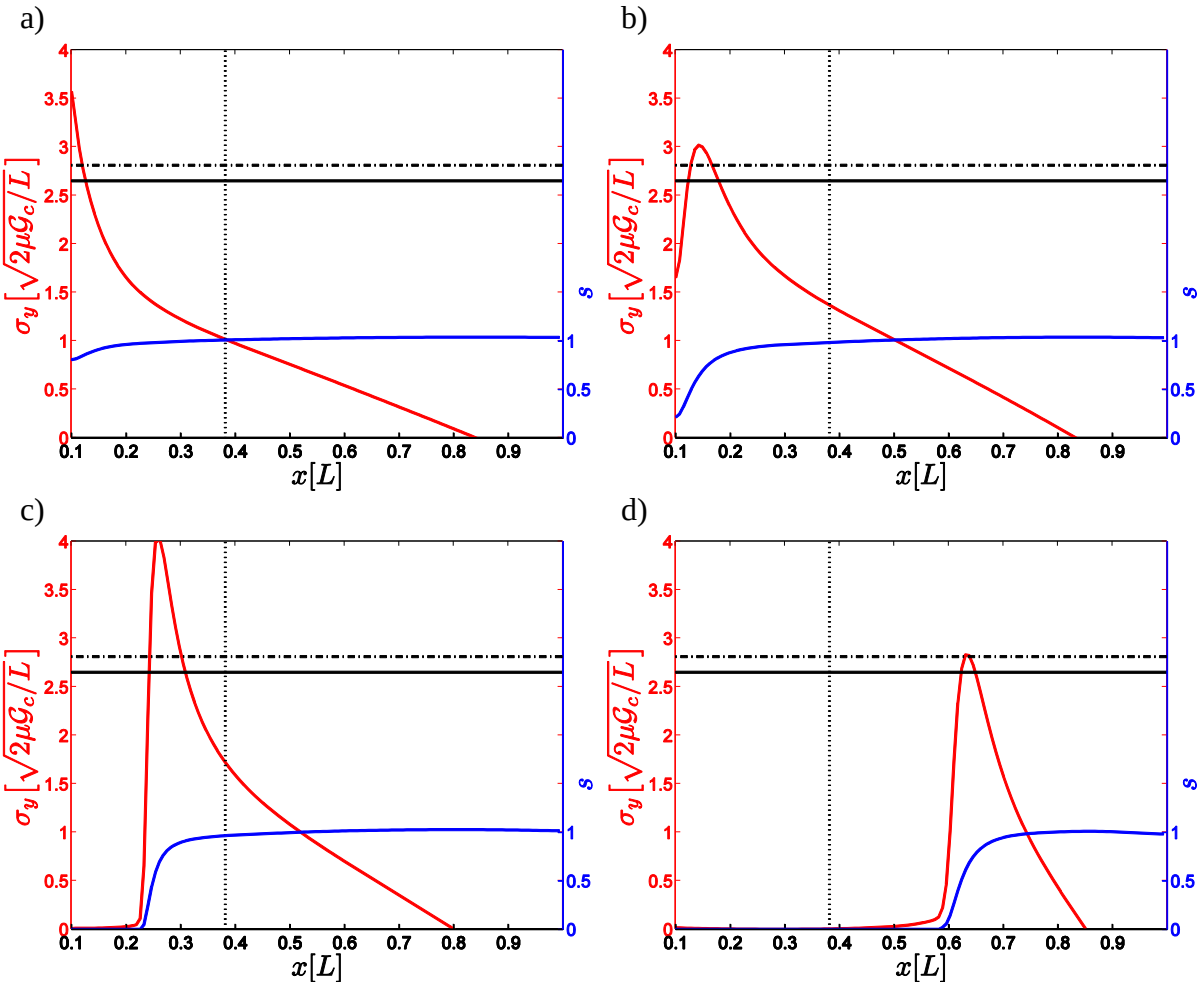

Figure 5. Stress in y-direction (red) and crack field (blue) along the x-axis at different load levels

The plots of Fig. 5 show the stress component σ_y (red) and the crack field s (blue) along the x-axis at the four load stages marked by the red circles in the right plot of Fig. 4. The vertical black dotted line marks the position of the crack tip after the formation of the initial crack. The horizontal black solid and dash-dotted lines indicate the strength estimates from Eq. (19) for the cases $i = 1$ and $i = 2$, respectively. At the load level of $u_0(t) = 0.7\sqrt{\mathcal{G}_c L/2\mu}$ (Fig. 5a), no crack nucleation is observed yet, and the numerical solution is stationary and stable. However, very close to the notch ground located at $x = 0.1L$, the stress component σ_y already exceeds the strength estimates. The value of the crack field at the notch ground is approximately $s \approx 0.80$, which is higher than the assumed critical value $s^* = 0.75$. Figure 5b) shows the y-stress and the crack field at the beginning of the phase of brutal crack nucleation at the load level $u_0(t) = 0.955\sqrt{\mathcal{G}_c L/2\mu}$. At this stage, the numerical solution becomes unstable and can no longer be considered as stationary. The crack field immediately at the notch ground is decreased to $s \approx 0.22$. Due to the loss of stiffness caused by the decreasing crack field, the stress at the notch ground decreases, too, and a stress peak develops in front of the notch. Figure 5c) shows the y-stress and crack field at $u_0(t) = 0.961\sqrt{\mathcal{G}_c L/2\mu}$, during the phase of brutal crack extension. The crack field has developed its characteristic exponential shape (cf. Eq. 15), where the material is not yet broken and is constantly zero in the fractured area. During this phase, the peak stress in y-direction significantly exceeds the maximal stress response (Eq. 19) of the homogeneous test problems. The last plot, Fig. 5d), shows the stress component σ_y and the crack field at $u_0(t) = 1.38\sqrt{\mathcal{G}_c L/2\mu}$, during the phase of stable crack extension. The peak stress is now in good agreement with the strength estimates. The crack field maintains its exponential shape and is only shifted in x-direction.

As similar results are obtained in simulations with different values of the length parameter ξ, the simulation results yield the following conclusions. For inhomogeneous stress states with maximum stresses below the derived strength estimates, no crack nucleation is observed in the phase field model. Also the exceedance of the assumed strength in a small area does not immediately lead to crack nucleation. Instead, an initial crack forms, if the stress becomes supercritical in a sufficiently large area and the crack field drops below the critical value of *0.75*. Thus, the derived strength estimates permit to judge the criticality of a computed stress state prior to crack nucleation and may therefore be interpreted as the effective fracture strength of the phase field model.

4. Conclusion and outlook

Despite the regularizing character of the length scale ξ, the stability analysis of the one dimensional model and the numerical results obtained for the two dimensional case, yield a more mechanically motivated interpretation of the parameter ξ. The stability analysis, as well as the numerical simulations, legitimate to interpret the maximal stress response obtained in homogeneous loading scenarios as the effective fracture strength σ_c of the phase field model. As a consequence of this interpretation, the length scale ξ is no longer just an arbitrary regularization length, but can be derived according to Eq. (19) from experimentally measurable data, i.e. from the cracking resistance $\mathcal{G}_c$, the fracture strength σ_c, and the Lamé constants λ and μ of isotropic materials. Thus, in conjunction with the other material parameters of the phase field model, the parameter ξ may be regarded as a material parameter itself. For the phase field formulation, the definition of the fracture strength, together with the ability to master the transition from a crack free initial state into a cracked configuration, justifies the conclusion, that the model naturally combines a strength criterion for the nucleation of new cracks with an energetically motivated Griffith type evolution law for stable crack growth.

The brutal formation of cracks of finite length at crack nucleation, observed in the simulations, challenges the limits of the quasi static formulation. Therefore, a dynamic version of the phase field model, where dynamic equations of motion replace the static equilibrium condition (Eq. 3), is currently being worked on. Within the context of the present work, especially the impact of the dynamic effects on the crack nucleation behavior of the phase field model is of interest. Another open task for future work is the influence of material inhomogeneities, such as inclusions or pores, on the effective fracture strength of the phase field model.

References

[1] I.S. Aranson, V.A. Kalatsky, V.M. Vinokur, Continuum field description of crack propagation. Phys Rev Let, 85/1 (2000) 118–121.
[2] L.O. Eastgate, J.P. Sethna, M. Rauscher, T. Cretegny, C.-S. Chen, C.R. Myers, Fracture in mode I using a conserved phase-field model. Phys Rev E, 65/3 (2002) 036117.
[3] A. Karma, A.E. Lobkovsky, Unsteady crack motion and branching in a phase-field model of brittle fracture. Phys Rev Let, 92/24 (2004) 245510.
[4] H. Henry, H. Levine, Dynamic instabilities of fracture under biaxial strain using a phase field model. Phys Rev Let, 93/10 (2004) 105504.
[5] V. Hakim, A. Karma, Crack path prediction in anisotropic brittle materials. Phys Rev Let, 95/23 (2005) 235501.
[6] F. Corson, M. Adda-Bedia, H. Henry, E. Katzav, Thermal fracture as a framework for quasi-static crack propagation. Int J Fract, 158 (2009) 1–14.
[7] B. Bourdin, G.A. Francfort, J.-J. Marigo, Numerical experiments in revisited brittle fracture. J Mech Phys Solid, 48/4 (2000) 797–826.
[8] C. Kuhn, R. Müller, A continuum phase field model for fracture. Eng Fract Mech, 77/18 (2010) 3625–3634.
[9] C. Miehe, F. Welschinger, M. Hofacker, Thermodynamically consistent phasefield models for fracture: Variational principles and multi-field FE implementations. Int J Numer Meth Eng, 83/10 (2010) 1273–1311.
[10] M.J. Borden, C.V. Verhoosel, M.A. Scott, T.J.R. Hughes, C.M. Landis, A phase-field description of dynamic brittle fracture. Comput Meth Appl Mech Eng, 217–220 (2012) 77–95.
[11] V. Hakim, A. Karma, Laws of crack motion and phase-field models of fracture. J Mech Phys Solid, 57/2 (2009) 342–368.
[12] C. Kuhn, R. Müller. On an energetic interpretation of a phase field model for fracture. PAMM, 11/1 (2011) 159–160.
[13] H. Amor, J.-J. Marigo, C. Maurini, N.K. Pham, Stability analysis and numerical implementation of non-local damage models via a global variational approach, in: WCCM8 - ECCOMAS 2008, 2008.
[14] K. Pham, H. Amor, J.-J. Marigo, C. Maurini, Gradient damage models and their use to approximate brittle fracture. Int J Damage Mech, 20/4 (2011) 618–652.
[15] K. Pham, J.-J. Marigo, and C. Maurini, The issues of the uniqueness and the stability of the homogeneous response in uniaxial tests with gradient damage models. J Mech Phys Solid, 59/6 (2011) 1163–1190.
[16] A. Benallal, J.-J. Marigo, Bifurcation and stability issues in gradient theories with softening. Modell Simul Mater Sci Eng, 15/1 (2007) 283–295.